Available online at www.sciencedirect.com
ScienceDirect
Trans. Nonferrous Met. Soc. China 34(2024) 2563−2574
Transactions of Nonferrous Metals Society of China
www.tnmsc.cn

Effect of brazing temperature on microstructure and tensile strength of γ-TiAl joint vacuum brazed with micro-nano Ti−Cu−Ni−Nb−Al−Hf filler

Li LI[1,2,3], Yu-tong CHEN[1,2], Lei-xin YUAN[1,2], Fen LUO[1,2], Zhi-xue FENG[1,2], Xiao-qiang LI[3]

1. School of Materials Science and Engineering, East China Jiaotong University, Nanchang 330013, China;
2. State Key Laboratory of Performance Monitoring and Protecting of Rail Transit Infrastructure, East China Jiaotong University, Nanchang 330013, China;
3. National Engineering Research Center of Near-net-shape Forming for Metallic Materials, South China University of Technology, Guangzhou 510640, China

Received 3 February 2023; accepted 18 August 2023

Abstract: A novel micro-nano Ti−10Cu−10Ni−8Al−8Nb−4Zr−1.5Hf filler was used to vacuum braze Ti−47Al−2Nb−2Cr−0.15B alloy at 1160−1220 °C for 30 min. The interfacial microstructure and formation mechanism of TiAl joints and the relationships among brazing temperature, interfacial microstructure and joint strength were emphatically investigated. Results show that the TiAl joints brazed at 1160 and 1180 °C possess three interfacial layers and mainly consist of α_2-Ti_3Al, τ_3-Al_3NiTi_2 and Ti_2Ni, but the brazing seams are no longer layered and Ti_2Ni is completely replaced by the uniformly distributed τ_3-Al_3NiTi_2 at 1200 and 1220 °C due to the destruction of α_2-Ti_3Al barrier layer. This transformation at 1200 °C obviously improves the tensile strength of the joint and obtains a maximum of 343 MPa. Notably, the outward diffusion of Al atoms from the dissolution of TiAl substrate dominates the microstructure evolution and tensile strength of the TiAl joint at different brazing temperatures.

Key words: γ-TiAl alloy; micro-nano filler; vacuum brazing; interfacial microstructure; tensile strength

1 Introduction

TiAl alloy is widely used in the automotive and aerospace fields due to its low density, high specific strength, excellent corrosion resistance and oxidation resistance at high temperatures, which has been considered as the most promising alternative material to replace Ni-based superalloys [1−3]. But the inherent characteristics of TiAl alloy, such as brittleness and poor workability, make the preparation of complicated or large-scale components very difficult [4−6]. Thus, it is necessary to choose a suitable connection method for TiAl alloy to widen its practical application. Among all joining methods, vacuum brazing has been considered as a superior connection method due to its convenience, cost-effectiveness, lower joining pressure requirement, high bonding quality and small deformation [7−9].

Compared with Ag-based and Al-based fillers, Ti-based fillers with higher melting temperature have better compatibility and wettability on TiAl alloys, so the TiAl joints brazed with them commonly possess high bonding strength, corrosion and oxidation resistance at ambient and elevated temperatures. Among the Ti-based fillers, the Ti−Zr−Cu−Ni system filler is widely used to braze TiAl alloy [10,11]. Cu and Ni are melting point depressant (MPD) elements in Ti-based filler and they are easy to form eutectic alloy with Ti, resulting in excellent wettability and flowability of

Corresponding author: Xiao-qiang LI, Tel/Fax: +86-20-87111080, E-mail: lixq@scut.edu.cn
DOI: 10.1016/S1003-6326(24)66560-X

filler over the surface of TiAl. However, overmuch brittle intermetallics (such as Ti_2Ni and Ti_2Cu) occur in the TiAl brazed joint due to the high content of Cu+Ni in the Ti−Zr−Cu−Ni filler, giving rise to the drop off in joint properties [11,12]. The melting temperature of Ti_2Cu/Ni is only about 1000 °C [13], which results in a low service temperature of the TiAl brazed joint. Therefore, the TiAl joint brazed with the Ti−Zr−Cu−Ni filler containing lower content of Cu and Ni should have superior bonding strength and high service temperature. As β-isomorphous element, Nb can form the infinite solid solution with Ti, addition of Nb into Ti alloy can significantly improve the mechanical properties (such as strength, toughness, and creep resistance) and oxidation resistance [14]. Al is a main element of the TiAl substrate, so addition of Al into Ti-based filler can improve the affinity and wettability of filler alloy with the TiAl substrate. The large atomic radius of Hf with similar chemical properties to Ti has a low diffusion rate in Ti-based alloy, the addition of Hf thus can improve the stability of the liquid phase and foil formation ability of Ti-based filler alloy, as well as refine its grain size [13]. Generally, the filler alloys with fine grain size possess lower segregation, more homogeneous and finer microstructure, larger specific surface area and better atomic activity, resulting in reduction of melting temperature for the filler alloy and enhancement of compositional homogeneity and interfacial reaction in the brazed joint, which is beneficial to obtaining a robust brazed joint [14]. Although micro-nano fabrication technology of Ti-based alloys has been greatly developed and perfected, few of the prepared alloys are selected as fillers to braze TiAl alloys.

Accordingly, we innovatively designed and prepared a novel multi-component micro-nano Ti−10Cu−10Ni−8Al−8Nb−4Zr−1.5Hf (wt.%) foil filler with low Cu and Ni contents to vacuum braze Ti−47Al−2Nb−2Cr−0.15B (at.%) alloy at 1160−1220 °C for 30 min. The formation mechanism of TiAl brazed joint and its interfacial microstructure evolution with brazing temperature as well as the internal relationship between the interfacial microstructure and tensile strength of TiAl brazed joint were systematically studied. Furthermore, the tensile fracture morphology was also analyzed to further investigate the variation of joint strength as a function of brazing temperature.

2 Experimental

The microstructure of Ti−47Al−2Nb−2Cr−0.15B (at.%) alloy used as parent metal displayed a lamellar characteristic consisting of γ-TiAl and α_2-Ti_3Al, as shown in Fig. 1. The casting filler alloy with a nominal composition of Ti−10Cu−10Ni−8Al−8Nb−4Zr−1.5Hf (wt.%) was vacuum arc remelted more than ten times in a water-cooled copper crucible. The prepared alloy ingot was produced into filler foil with a thickness of about 80 μm and a width of 5−6 mm by induction melting first and then single roller melt-spinning technique. The microstructures and element distributions of casting and foil fillers were characterized by scanning electron microscope (SEM) equipped with energy dispersive spectrometer (EDS). And their phase constitutions were further verified by X-ray diffractometer (XRD) and transmission electron microscopy (TEM) with selected area electron diffraction (SAED). Meanwhile, differential scanning calorimetry (DSC) was carried out for the casting and foil fillers at a heating rate of 20 °C/min.

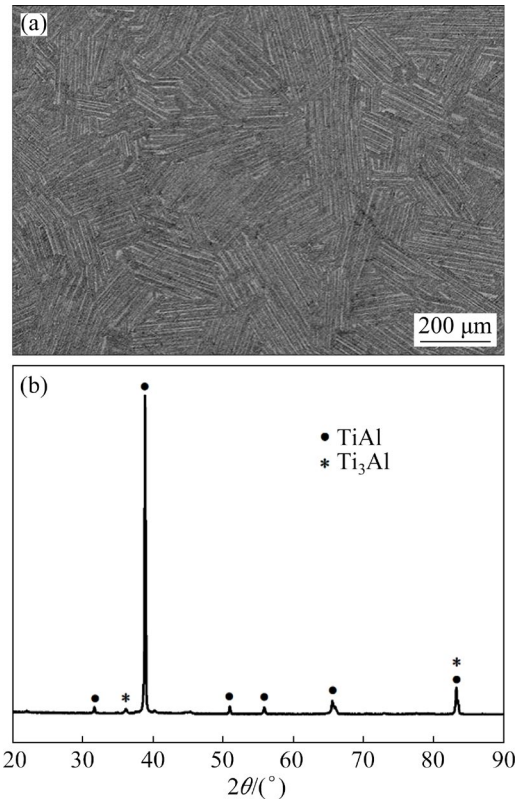

Fig. 1 Microstructure (a) and XRD pattern (b) of Ti−47Al−2Nb−2Cr−0.15B parent metal

Prior to brazing, the joining surfaces of TiAl parent metal and filler foil were polished by metallographic sandpaper with grit sizes from 180# to 1500#, and then ultrasonically cleaned in acetone for 5 min. The eventual size of the filler foil for brazing was 13 mm in length, 5−6 mm in width, and 60 μm in thickness, which was sandwiched between two TiAl alloys, as shown in Fig. 2(a). The brazing experiment was performed in an HP-12 × 12 × 12 vacuum furnace with a vacuum degree of ~13.3 mPa. The brazing temperature ranged from 1160 to 1220 °C for 30 min and the corresponding schematic diagram of the temperature profile for brazing is shown in Fig. 2(b). The TiAl brazed joints were cut into tensile and metallographic specimens according to the schematic diagram, as shown in Fig. 2(c). The room temperature (RT) tensile strength of TiAl brazed joints was evaluated by an AG-X100KN universal testing machine at a constant speed of 0.5 mm/min. SEM and EDS were employed to characterize the interfacial microstructures of the TiAl brazed joints and their fracture morphologies after tensile test.

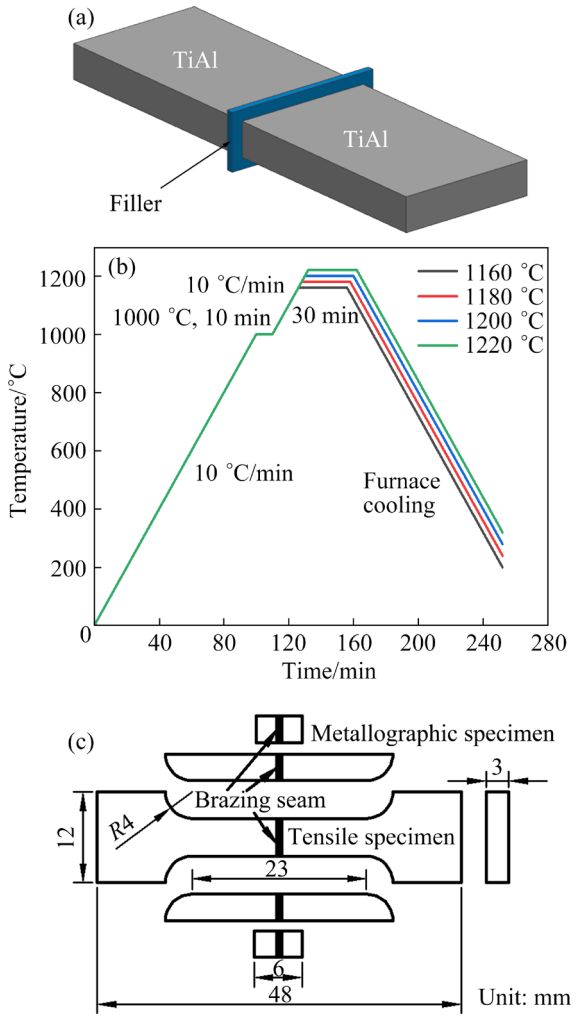

Fig. 2 Schematic diagrams: (a) Assembly for brazing; (b) Temperature profile for brazing; (c) Specimens for tensile test and metallographic examination

3 Results and discussion

3.1 Microstructures of Ti−Cu−Ni−Al−Nb−Zr−Hf fillers

Figures 3(a) and (c) show the backscattered electron images (BEIs) of the casting and foil Ti−Cu−Ni−Al−Nb−Zr−Hf fillers. It is clearly seen that the microstructure of casting filler shows three obvious contrasts, marked as *A*, *B* and *C* in Fig. 3(a). According to the EDS results (Table 1) and Refs. [10,15], it can be inferred that the black block Zone *A* is primarily α_2-Ti_3Al, the gray Zone *B* is $Ti_2Cu(Ni)$ and the dark gray block Zone *C* is $Ti_2Cu(Ni)$ + α_2-Ti_3Al. This is further confirmed by the XRD pattern in Fig. 3(b). Meanwhile, it can be observed that the foil filler reveals a featureless contrast (Fig. 3(c)), indicating that the element distribution of the foil filler is uniform, which is further verified by the EDS results of Zones *D*–*F* (see Table 1). The bright field TEM image of the foil filler (Fig. 3(d)) reveals that the grain size of the foil filler is in the range of 50−300 nm and belongs to micro-nanocrystalline characteristics. In general, the uniform composition and fine microstructure of the filler alloy are beneficial to shortening its melting interval, thereby improving its brazeability [16].

Figure 4 shows the DSC curves of casting and micro-nano fillers. The melting ranges of the casting and micro-nano fillers are 1128.57−1161.44 °C and 1134.73−1155.43 °C, respectively. Apparently, the melting range of the micro-nano filler foil is narrower than that of the casting filler, and the liquidus temperature (T_L) of the micro-nano filler foil is lower than that of the casting filler, which further proves that the uniform composition of filler alloy is beneficial to shortening the melting interval. It is well known that the narrower melting range and lower T_L of the filler are beneficial to reducing the formation of voids or cracks in the brazed joints and obtaining robust joints [16]. Therefore, we selected micro-nano filler to vacuum braze Ti−47Al−2Nb−2Cr−0.15B (at.%) alloy.

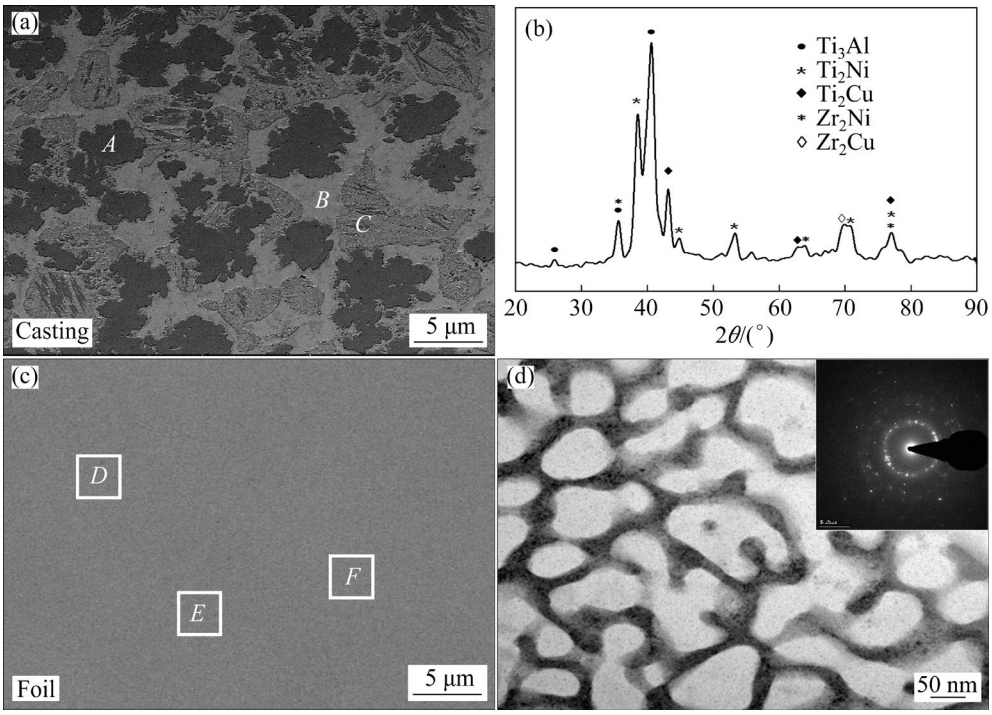

Fig. 3 Backscattered electron images (BEIs) of Ti−Cu−Ni−Al−Nb−Zr−Hf fillers (a, c), XRD pattern of Ti−Cu−Ni−Al−Nb−Zr−Hf casting filler (b), and bright field TEM image with corresponding SAED pattern of Ti−Cu−Ni−Al−Nb−Zr−Hf foil filler (d)

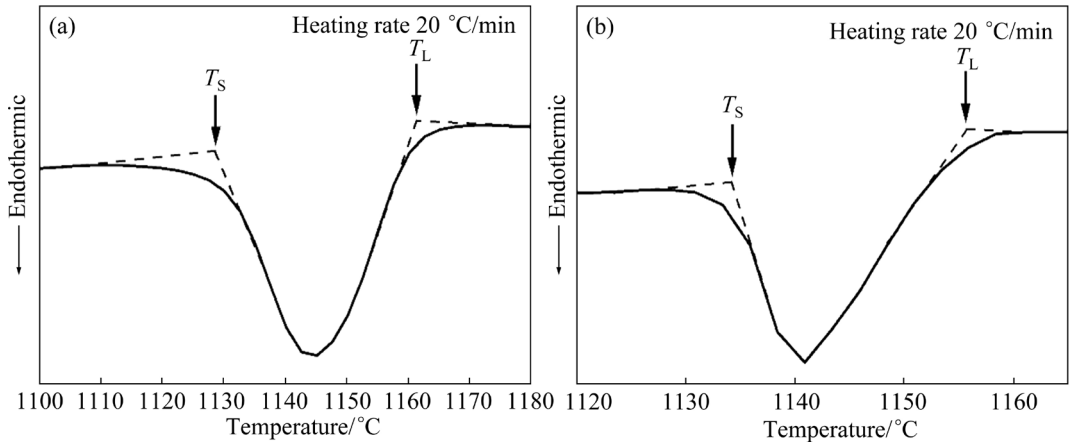

Fig. 4 DSC curves of Ti−Cu−Ni−Al−Nb−Zr−Hf: (a) Casting; (b) Micro-nano foil fillers

Table 1 EDS results of each zone in Figs. 3(a, c)

Zone	Content/at.%							Possible phase
	Ti	Al	Zr	Ni	Cu	Nb	Hf	
A	70.83	22.57	0.92	1.12	1.33	2.65	0.58	α_2-Ti_3Al
B	55.71	4.48	3.60	16.95	13.90	4.92	0.44	Ti_2Cu(Ni)
C	63.59	10.52	1.88	7.92	11.72	4.02	0.35	Ti_2Cu(Ni)+ α_2-Ti_3Al
D	61.62	14.99	2.06	8.66	7.95	4.28	0.44	−
E	61.52	14.96	2.17	8.52	8.01	4.40	0.42	−
F	61.57	14.87	2.26	8.59	7.98	4.30	0.43	−

Generally, the selected brazing temperature should be higher than the liquidus temperature of the filler to ensure that the filler is completely melted. Accordingly, the Ti−Cu−Ni−Al−Nb−Zr−Hf micro-nano filler foil was used to vacuum braze TiAl alloy at 1160−1220 °C in the following study.

3.2 Interfacial microstructure of TiAl joint brazed with micro-nano Ti−Cu−Ni−Al−Nb−Zr−Hf filler foil

Figure 5 shows the interfacial microstructure of the TiAl joint brazed at 1180 °C for 30 min. It can be clearly seen that there are no cracks or pores,

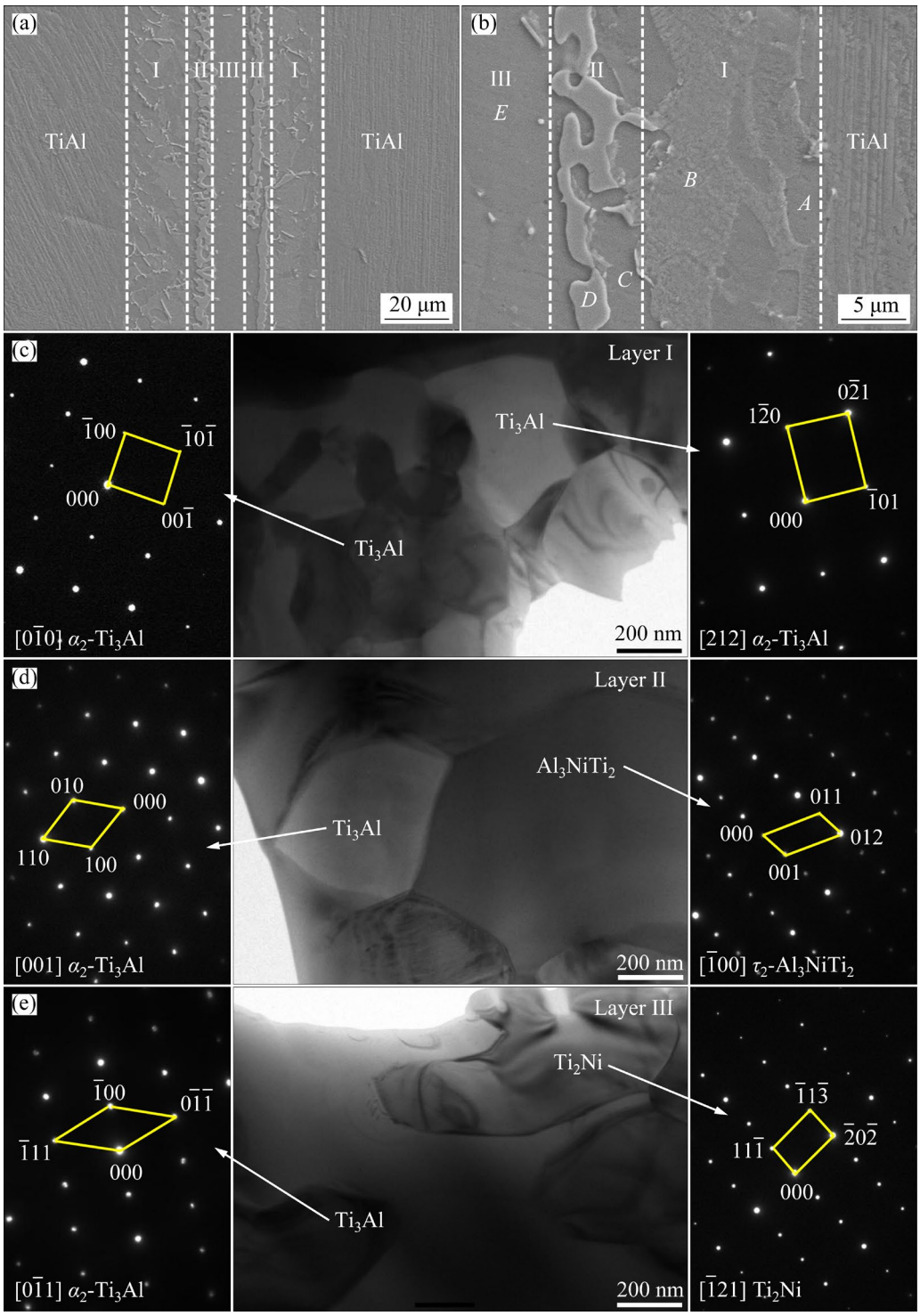

Fig. 5 Interfacial microstructure of TiAl joint brazed at 1180 °C for 30 min: (a, b) Whole joint and high magnification of brazing seam, respectively; (c, d, e) Bright field TEM images with corresponding SAED patterns of Layer I, Layer II and Layer III, respectively

indicating that the brazed joint is soundly bonded. The total width of the brazing seam is about 73 μm, which is 21.7% higher than that of the original filler foil, demonstrating that intensive interfacial reaction has taken place between the filler alloy and TiAl substrate. Based on the interfacial morphology of the TiAl brazed joint, it can be divided into solid diffusion Layer I, isothermal solidification Layer II and central brazed Layer III, as shown in Fig. 5(a). The high magnification of the brazing seam is shown in Fig. 5(b). According to the contrast difference, Layer I mainly consists of Phases *A* and *B*, Layer II is mixed with two different phases (Phase *C* and Phase *D*) and Phase *E* occupies Layer III. Zr and Hf as neutral element of Ti and Nb as isomorphous element of *β*-Ti, all of them can form infinite solid solution with Ti, so Zr, Nb and Hf to a certain extent can be regarded as element Ti [17]. Cu and Ni are *β*-Ti active eutectoid elements with similar atomic size and crystal structure, they are chemically compatible with and fully soluble to each other [18]. According to the Cr−Ni binary diagram [19], the maximum solid solubility of Cr in Ni is more than 22 at.%. Therefore, Cu, Cr and Ni in a certain sense are collectively referred to as Ni in the following discussion. Combining the EDS analysis results listed in Table 2, Ti−Ni−Al ternary alloy phase diagram [20] and the research results reported by REN et al [21], it can be deduced that Phase *A* is mainly α_2-Ti_3Al with minor *γ*-TiAl, Phases *B* and *C* are α_2-Ti_3Al, Phase *D* is τ_3-Al_3NiTi_2, and Phase *E* is α_2-Ti_3Al + Ti_2Ni, which are further verified by the bright field TEM images with the corresponding SAED patterns (Figs. 5(c−e)) of Layers I, Layer II and Layer III, respectively.

Due to driving by the concentration gradients, Al atoms diffuse outwards from the TiAl parent metal and the filler atoms (Ti, Zr, Cu, Ni and Hf) as melting point depressants diffuse into the TiAl parent metal, resulting in formation of solid diffusion Layer I and dissolution of the TiAl parent metal into the molten filler. The concentration of Al decreases but that of Ti increases in Layer I and makes the molar ratio of Ti to Al satisfy the formation compositional (molar ratio 1.5−3.2 [22]) of α_2-Ti_3Al, the original *γ*-TiAl is thus transformed into α_2-Ti_3Al (marked as *A* and *B* in Fig. 5(b)). The bright field TEM image with the corresponding SAED patterns (Fig. 5(c)) indicates that only α_2-Ti_3Al exists without *γ*-TiAl in the Layer I, which may be attributed to complete transformation of *γ*-TiAl into α_2-Ti_3Al or the TEM sample taken from the outer part of Layer I adjacent to Layer II. The inner part of the dissolution of TiAl parent metal makes the liquidus temperature of the Ti−Cu−Ni−Al−Nb−Zr−Hf filler alloy increase to the brazing temperature or above, which mixes with the molten filler and forms isothermal solidification Layer II, and the outer part will diffuse toward the central brazing seam in the molten filler and distribute in the Layer III. Epitaxial solidification occurs in the Layer II closed to the Layer I, so Phase *C* should be the same as Phase *B*, which is further verified by the EDS result in Table 2 and both are α_2-Ti_3Al. As can be seen in Fig. 5(b), a large continuous α_2-Ti_3Al layer is formed by Phases *B* and *C*, which acts as a barrier to obstruct the atomic inter-diffusion between its two sides. The same phenomenon is also found by REN et al [21] and they pointed out that the successive diffusion of filler atoms (especially Ni and Cu) towards TiAl substrate is restrained by the α_2-Ti_3Al barrier. Therefore, Cu and Ni enrich in the outer part of Layer II and form Phase *D*. According to the EDS result (Table 2) of Phase *D* and the research results reported by ZENG et al [23], Ti, Ni and Al are the main elements and they are in the compositional

Table 2 EDS results of each phase in Fig. 5(b)

Phase	Content/at.%								Possible phase
	Ti	Al	Ni	Cu	Nb	Zr	Cr	Hf	
A	55.93	36.79	0.37	1.00	2.82	0.11	2.87	0.11	α_2-Ti_3Al+*γ*-TiAl
B	65.57	24.68	1.47	2.55	2.59	0.87	2.17	0.10	α_2-Ti_3Al
C	71.97	23.67	0.29	0.91	2.04	0.12	0.83	0.17	α_2-Ti_3Al
D	39.54	32.14	12.46	9.38	1.95	2.81	0.69	1.03	τ_3-Al_3NiTi_2
E	58.87	24.44	6.87	5.69	3.14	0.43	0.37	0.19	α_2-Ti_3Al+Ti_2Ni

range of τ_3-Al_3NiTi_2 varied from $Al_{30}Ni_{28}Ti_{42}$ (at.%) to $Al_{50}Ni_{16}Ti_{34}$ (at.%), Phase *D* is thus determined as τ_3-Al_3NiTi_2 exhibited the structure of $MgZn_2$. An interesting phenomenon is found in the high magnification SEM of the brazing seam and the bright field TEM image of Layer II (Figs. 5(b, d)) that rounded boundaries occurred between α_2-Ti_3Al and τ_3-Al_3NiTi_2. Similar phenomenon is also found by RASTKAR and SOHI [24] and they explained that the stable phase of τ_3-Al_3NiTi_2 nucleated first together with low surface tension grains of α_2-Ti_3Al and then α_2-Ti_3Al grains wetted the grain boundaries of τ_3-Al_3NiTi_2 phase and partly dissolved τ_3-Al_3NiTi_2. The diffusion of Al from the TiAl substrate increases the content of Al in the Layer III and dilutes the concentration of filler elements, while the diffusion of filler elements towards TiAl substrate also decreases their concentrations in Layer III, resulting in increase of α_2-Ti_3Al and reduction of Ti_2Ni in Layer III. The above conclusion is further proved by the EDS result of Phase *E* occupied the Layer III and the proportion of α_2-Ti_3Al is more than that of Ti_2Ni, which is contrary to their proportions in the original crystalline Ti−Cu−Ni−Al−Nb−Zr−Hf filler. Notably, it seems that the corresponding SEM image of Phase *E* reveals a featureless contrast (Fig. 5(b)), indicating that its element distribution and microstructure are uniform. The bright field TEM image with the corresponding SAED patterns of the Layer III determines that Phase *E* has two different phases of α_2-Ti_3Al and Ti_2Ni rather than only one phase.

Figure 6 shows the interfacial microstructure of TiAl joints brazed at different temperatures for 30 min. It can be seen that the thickness of the brazing seam increases first and then decreases with brazing temperature, which may be attributed to the increase of element diffusion coefficient and fluidity of liquid filler. The thickness of the brazing seam is only 70 μm at the brazing temperature of 1160 °C, which is slightly thicker than that of the origin filler foil. The main cause may be a low atomic diffusion coefficient and insufficient interaction between the parent metal and the filler at a lower temperature. The Arrhenius equation ($D=D_0\exp(-Q(RT)^{-1})$) [25] indicates that the atomic diffusion coefficient (D) increases with increasing temperature (T). Generally, increasing the brazing temperature can increase the fluidity of the molten filler, the dissolution of the parent metal into the molten filler pool and the diffused depth of the filler atoms into the parent metal [26]. Therefore, the thickness of the brazing seam gradually increases when the brazing temperature increases from 1160 to 1200 °C, as shown in Figs. 6(a−c). However, the

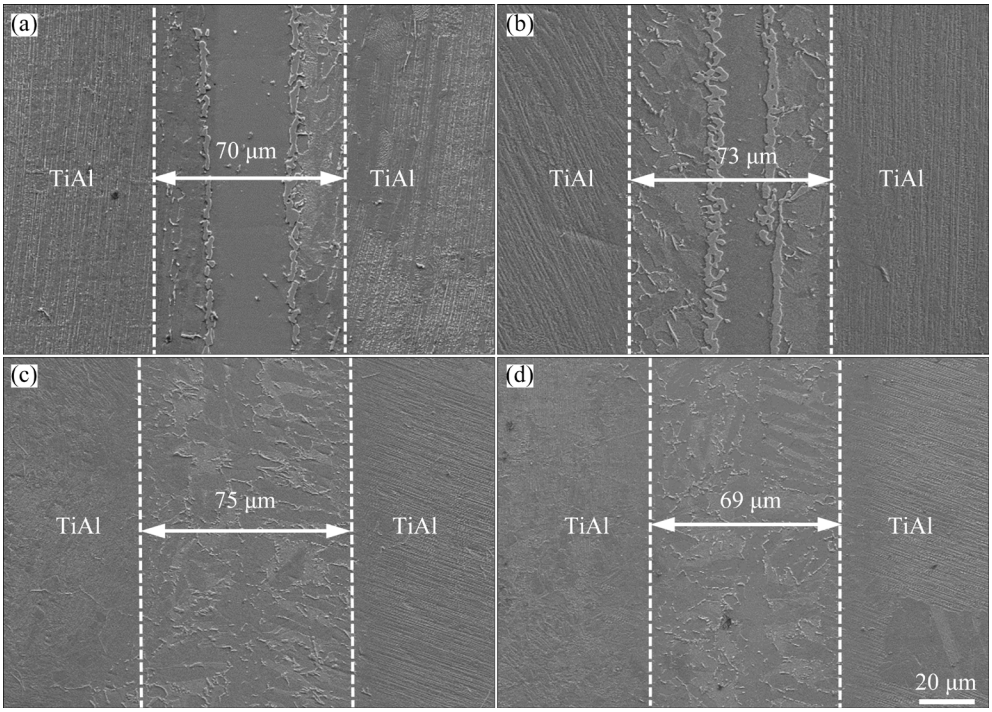

Fig. 6 Interfacial microstructures of TiAl joints brazed at 1160 °C (a), 1180 °C (b), 1200 °C (c) and 1220 °C (d) for 30 min

thickness of the brazing seam reversely decreases when the brazing temperature is further increased to 1220 °C. It may be imputed to the liquid filler losses from the gap between the two parent metals due to the extremely excellent fluidity of the filler alloy at a high temperature. Accordingly, the maximum thickness of the brazing seam is 75 μm obtained at 1200 °C.

There are obvious three regular and well-demarcated layers of the joints brazed at 1160 and 1180 °C, as shown in Figs. 6(a, b). The thickness of the solid diffusion Layer I and isothermal solidification Layer II increases but that of the central brazed Layer III decreases with increasing brazing temperature, it is further indicated that the dissolution of TiAl substrate into the molten filler as well as interdiffusion and interaction between both of them is enhanced with brazing temperature. However, it is hard to distinguish the boundary between Layers I and II as well as Layers II and III once the brazing temperature is up to 1200 °C or above, as shown in Figs. 6(c, d). Similar phenomenon is also found by LEE and WU [27], they pointed out that α_2-Ti_3Al became unstable and the successive α_2-Ti_3Al barrier layer was broken once the temperature was up to 1200 °C or above, resulting in sharp increase of dissolution of TiAl substrate and more sufficient atomic interdiffusion and metallurgical reaction between TiAl parent alloy and filler alloy.

Owing to the existence of the large continuous α_2-Ti_3Al layer formed on both sides of the boundary between Layer I and Layer II, the atomic inter-diffusion between its two sides is obstructed. So the increasing diffusion of Al into the central brazed Layer III with increasing brazing temperature from 1160 to 1180 °C brings about increase of α_2-Ti_3Al but reduction of Ti_2Ni in Layer III. Meanwhile, the constitution and distribution of the phases in Layers I and II are almost unchanged. Further increasing the brazing temperature to 1200 and 1220 °C, the successive α_2-Ti_3Al barrier layer is broken and a large amount of Al sharply diffuses into the central brazed Layer III and increases with brazing temperature, leading to entire replacement of Ti_2Ni with τ_3-Al_3NiTi_2. τ_3-Al_3NiTi_2 increases but α_2-Ti_3Al decreases with brazing temperature. Accordingly, Al is the main controlling factor pertaining to the microstructure evolution of TiAl brazed joints. The microstructure morphology and the content and distribution of each phase in the brazing seams can be regulated by adjusting Al from the dissolution of TiAl substrate to further improve the bonding quality of TiAl brazed joint.

3.3 Evaluation of tensile strength and fracture analysis of TiAl brazed joints

Figure 7 shows the room temperature (RT) tensile strength of TiAl joints brazed at different temperatures for 30 min. The tensile strength of the TiAl brazed joint increases first and then decreases with brazing temperature, and the maximum tensile strength of 343 MPa is obtained at 1200 °C. As can be seen from Figs. 6 and 7, the variation of joint strength as a function of brazing temperature is largely dependent upon the interfacial micro-structure morphology and the content and distribution of each phase in the TiAl brazed joint. Noticeably, the joint strength variation is consistent with the thickness variation of the brazing seam. The tensile strength of the TiAl brazed joint increases from 175 MPa at 1160 °C to 229 MPa at 1180 °C. One reason is that the lower dissolution of TiAl substrate in the molten filler as well as weaker inter-diffusion and metallurgical combination reaction between both of them occurs at low brazing temperature and increases with brazing temperature. Another reason may be that high hardness Ti_2Ni (HV 700 [28]) decreases but low hardness α_2-Ti_3Al (HV 341.6 [28]) increases with increasing brazing temperature from 1160 to 1180 °C in Layer III, which can release residual stresses of the brazing seam to a certain extent and improve the joint strength. When the brazing temperature is increased up to 1200 °C, the continuous

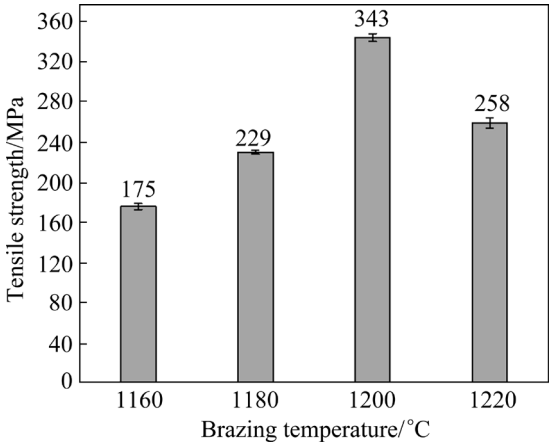

Fig. 7 RT tensile strength of TiAl joints brazed at different temperatures for 30 min

α_2-Ti_3Al barrier layer is broken and sufficient inter-diffusion and metallurgical combination reaction occur between TiAl substrate and filler alloy, resulting in sufficiently uniform distribution of τ_3-Al_3NiTi_2 and α_2-Ti_3Al in the whole brazing seam and transformation from three interfacial layers at 1180 °C to one interfacial layer at 1200 °C. This is beneficial to decreasing the difference in thermal expansion coefficient and residual stress in the brazing seam and improving the joint strength. Meanwhile, the maximum hardness of τ_3-Al_3NiTi_2 (HV 1749.3 [29]) enriches the outer part of Layer II adjacent to Layer III at brazing temperatures of 1160 and 1180 °C, resulting in obtaining a lower joint strength. Therefore, the tensile strength of the joint brazed at 1200 °C significantly increases by almost 50%, reaching 343 MPa. Further increasing the brazing temperature to 1220 °C, increase of τ_3-Al_3NiTi_2 and reduction of α_2-Ti_3Al embrittle the brazing seam and make thermal stress difficult to release, while overmuch residual thermal stress also will yield in the TiAl joint brazed at high temperature, resulting in reverse reduction of the tensile strength to 258 MPa. Accordingly, the content and distribution of τ_3-Al_3NiTi_2 are the key factors to the joint strength, and it should be avoided accumulation or overmuch in the brazing seam to obtain a robust joint.

Figure 8 shows the fracture morphologies of TiAl joints brazed at different temperatures for 30 min after tensile test. All TiAl brazed joints have obvious cleavage facets and typical brittle cleavage fracture characteristics. The EDS analysis results listed in Table 3 and XRD patterns (Figs. 8(e, f))

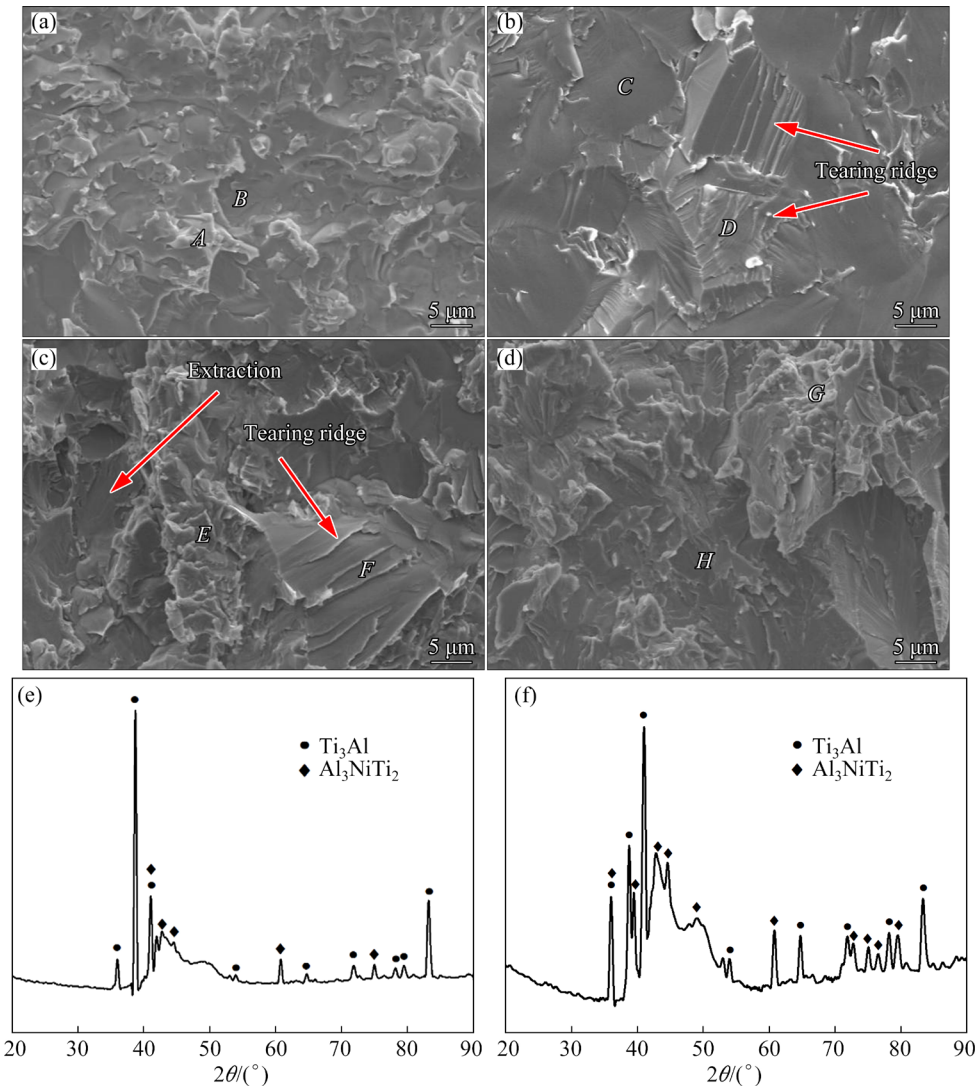

Fig. 8 Fracture morphologies of TiAl joints brazed at different temperatures for 30 min after tensile test (a−d) and corresponding XRD patterns at brazing temperatures of 1180 °C (e) and 1200 °C (f), respectively: (a) 1160 °C; (b) 1180 °C; (c) 1200 °C; (d) 1220 °C

Table 3 EDS results of fracture surfaces in Fig. 8

Position	Content/at.%							Possible phase
	Ti	Al	Ni	Zr	Nb	Cu	Cr	
A	34.57	40.21	18.81	3.59	0.97	1.04	0.45	τ_3-Al_3NiTi_2
B	67.93	24.40	0.45	4.06	1.63	1.21	0.32	α_2-Ti_3Al
C	69.52	26.09	0.10	0.34	3.22	0.23	0.58	α_2-Ti_3Al
D	35.34	40.37	20.27	0.28	2.53	0.50	0.72	τ_3-Al_3NiTi_2
E	35.29	40.49	20.12	0.09	2.26	0.84	0.91	τ_3-Al_3NiTi_2
F	65.19	29.52	0.39	0.00	2.21	0.55	2.15	α_2-Ti_3Al
G	41.74	35.08	19.41	0.14	2.10	0.71	0.82	τ_3-Al_3NiTi_2
H	67.29	28.65	0.18	0.19	2.32	0.60	0.77	α_2-Ti_3Al

indicate that only brittle τ_3-Al_3NiTi_2 and α_2-Ti_3Al exist on the fracture surface corresponding to each brazing temperature. Therefore, it can be inferred that the failures take place in the isothermal solidification Layer II of the TiAl joints brazed at 1160 and 1180 °C. It is worth mentioning that obvious tearing ridges are found on the fracture surfaces at brazing temperatures of 1180 and 1200 °C (Figs. 8(b, c), indicating that the tensile strength of the TiAl joint brazed at 1180 and 1200 °C should be higher than that at 1160 and 1220 °C, respectively. The fracture surface at brazing temperature of 1200 °C is the roughest and even contains large particle extraction similar to dimple. In general, the rough fracture surface forms along with large particles pull-out and needs to overcome significant increase of fracture energy, and the alloy possesses better mechanical properties [30,31]. Therefore, the maximum tensile strength of the TiAl joint is obtained at 1200 °C. The aforementioned results are consistent with the variation of the tensile strength of TiAl brazed joints as a function of brazing temperature in Fig. 7.

4 Conclusions

(1) Compared with the casting filler containing α_2-Ti_3Al, $Ti_2Cu(Ni)$ and $Ti_2Cu(Ni)$ + Ti_3Al, the foil filler with uniform element distribution is verified as typical micro-nano crystalline characteristics and possesses narrower melting interval and lower liquidus temperature. The Ti−Cu−Ni−Al−Nb−Zr−Hf micro-nano filler foil is used to vacuum braze Ti−47Al−2Nb−2Cr−0.15B (at.%) alloy at 1160−1220 °C for 30 min. The typical interfacial microstructure of γ-TiAl brazed joint is TiAl/α_2-Ti_3Al + TiAl (Layer I)/α_2-Ti_3Al + τ_3-Al_3NiTi_2 (Layer II)/Ti_2Ni + α_2-Ti_3Al (Layer III)/α_2-Ti_3Al + τ_3-Al_3NiTi_2 (Layer II)/α_2-Ti_3Al + TiAl (Layer I)/TiAl.

(2) Regular TiAl brazing seams with obvious three-layers are presented at brazing temperatures of 1160 and 1180 °C, but no obvious multi-layer exists at 1200 and 1220 °C. Once the brazing temperature is up to 1200 °C, Ti_2Ni is completely replaced of τ_3-Al_3NiTi_2 due to the disappearance of the successive α_2-Ti_3Al barrier layer and excessive increasing diffusion of Al into the central brazed Layer III, indicating that the interfacial microstructure of TiAl brazed joint is dependent on the diffusion of Al from the dissolution of TiAl substrate.

(3) The RT tensile strength of the TiAl brazed joint increases first and then decreases with increasing brazing temperature and the maximum tensile strength of 343 MPa is obtained at 1200 °C. The variation of tensile strength is closely related to the microstructure evolution of Ti_2Ni, τ_3-Al_3NiTi_2 and α_2-Ti_3Al with brazing temperature. Notably, the content and distribution of τ_3-Al_3NiTi_2 are the key factors to the joint strength. The tensile fracture of TiAl brazed joints exhibits obvious cleavage regardless of brazing temperatures and all cracks prefer to nucleate and propagate between α_2-Ti_3Al and τ_3-Al_3NiTi_2.

CRediT authorship contribution statement

Li LI: Conceptualization, Methodology, Investigation, Resources, Writing − Original draft, Writing − Review & editing, Funding acquisition; **Yu-tong CHEN:** Formal analysis, Data curation, Writing − Original draft, Writing − Review & editing,

Visualization; **Lei-xin YUAN:** Data curation, Writing − Review & editing; **Fen LUO:** Data curation, Writing − Review & editing; **Zhi-xue FENG:** Validation, Investigation, Writing − Original draft; **Xiao-qiang LI:** Supervision, Funding acquisition.

Declaration of competing interest

The authors declare that they have no known competing financial interests or personal relationships that could have appeared to influence the work reported in this paper.

Acknowledgments

This work was supported by the National Natural Science Foundation of China (No. 51865012), the Natural Science Foundation of Jiangxi Province, China (No. 20202BABL204040), the Open Foundation of National Engineering Research Center of Near-net-shape Forming for Metallic Materials, China (No. 2016005), the Science Foundation of Educational Department of Jiangxi Province, China (No. GJJ170372), the GF Basic Scientific Research Project, China (No. JCKY2020205C002), and the Civil Population Supporting Planning and Development Project, China (No. JPPT125GH038).

References

[1] YANG Ying-fei, XIAO Qin, REN Pan, LI Wei, ZHU Sheng-long, WANG Fu-hui. Improved oxidation resistance of γ-TiAl intermetallics by sputtered Ni+CrAlYHfSiN composite coating [J]. Corrosion Science, 2021, 187: 109510.

[2] XU Run-run, LI Miao-quan, ZHAO Yong-hao. A review of microstructure control and mechanical performance optimization of γ-TiAl alloys [J]. Journal of Alloys and Compounds, 2023, 932: 167611.

[3] LI Ming-ao, LI Juan, ZHOU Tao, HU Li, SHI Lai-xin, CHEN Yu-yong, XU Li-juan, XIAO Shu-long. Microstructure evolution, deformation behavior and manufacture design of TiAl matrix composites reinforced with in-situ borides precipitation [J]. Transactions of Nonferrous Metals Society of China, 2023, 33: 107−127.

[4] JIANG Min-jin, SUN Hong-liang, LIU Rui, JIANG Xiao-song, ZHANG Ya-li, SUN Da-ming. Fabrication and mechanical properties of Ti_2AlN/TiAl composite with continuous network structure [J]. Transactions of Nonferrous Metals Society of China, 2023, 33: 1437−1451.

[5] ZHAI Wen-gang, WANG Pan, NG F L, ZHOU Wei, NAI S M L, WEI Jun. Hybrid manufacturing of γ-TiAl and Ti−6Al−4V bimetal component with enhanced strength using electron beam melting [J]. Composites Part B: Engineering, 2021, 207: 108587.

[6] CAO Jian, DAI Xiang-yu, LIU Jia-qi, SI Xiao-qing, FENG Ji-cai. Relationship between microstructure and mechanical properties of TiAl/Ti_2AlNb joint brazed using Ti−27Co eutectic filler metal [J]. Materials & Design, 2017, 121: 176−184.

[7] DONG Hong-gang, ZHANG Run-ze, XIA Yue-qing, HAO Xiao-hu, LI Peng. Interfacial features of TiAl alloy/316L stainless steel joint brazed with Zr−Cu−Ni−Al amorphous filler metal [J]. Transactions of Nonferrous Metals Society of China, 2021, 31: 1680−1688.

[8] CAI Yu-sheng, LIU Ren-ci, JI H B, CUI Yu-you, YANG R. Vacuum brazing TiAl-based intermetallics using novel Ti−Fe−Mn eutectic brazing alloy [J]. Intermetallics, 2021, 136: 107274.

[9] NIU Guo-bin, WANG Dong-po, YANG Zhen-wen, WANG Ying. Microstructure and mechanical properties of Al_2O_3 ceramic and TiAl alloy joints brazed with Ag−Cu−Ti filler metal [J]. Ceramics International, 2016, 42: 6924−6934.

[10] LI Xiao-qiang, LI Li, HU Ke, QU Sheng-guan. Vacuum brazing of TiAl-based intermetallics with Ti−Zr−Cu−Ni−Co amorphous alloy as filler metal [J]. Intermetallics, 2015, 57: 7−16.

[11] QIU Qi-wen, WANG Ying, YANG Zhen-wen, HU Xin, WANG Dong-po. Microstructure and mechanical properties of TiAl alloy joints vacuum brazed with Ti−Zr−Ni−Cu brazing powder without and with Mo additive [J]. Materials & Design, 2016, 90: 650−659.

[12] LI Li, ZHAO Wei, FENG Zhi-xue, SUN Jia, LI Xiao-qiang. Microstructure and shear strength of γ-TiAl/GH536 joints brazed with Ti−Zr−Cu−Ni−Fe−Co−Mo filler alloy [J]. Transactions of Nonferrous Metals Society of China, 2020, 30: 2143−2155.

[13] LEYENS C, PETERS M. Titanium and titanium alloys [M]. New York: Wiley-VCH, 2003.

[14] IMAYEV V M, GANEEV A A, TROFIMOV D M, PARKHIMOVICH N J, IMAYEV R M. Effect of Nb, Zr and Zr + Hf on the microstructure and mechanical properties of β-solidifying γ-TiAl alloys [J]. Materials Science and Engineering: A, 2021, 817: 141388.

[15] LIU Shi-lei, MIAO Jia-kai, ZHANG Wei-wei, WEI Ran, CHEN Chen, WANG Tan, ZHAO Wu-duo, JIANG Zheng-yi, LI Fu-shan. Interfacial microstructure and shear strength of TC4 alloy joints vacuum brazed with Ti−Zr−Ni−Cu filler metal [J]. Materials Science and Engineering: A, 2020, 775: 138990.

[16] LI Li, LI Xiao-qiang, HU Ke, HE Bo-lin, MAN Hua. Brazeability evaluation of Ti−Zr−Cu−Ni−Co−Mo filler for vacuum brazing TiAl-based alloy [J]. Transactions of Nonferrous Metals Society of China, 2019, 29: 754−763.

[17] ZHU Li-long, ZHANG Qiao-fu, CHEN Zhang-qi, WEI Chang-dong, CAI Ge-mei, JIANG Liang, JIN Zhan-peng, ZHAO Ji-cheng. Measurement of interdiffusion and impurity diffusion coefficients in the bcc phase of the Ti−X (X = Cr, Hf, Mo, Nb, V, Zr) binary systems using diffusion multiples [J]. Journal of Materials Science, 2017, 52: 3255−3268.

[18] LEE M K, KIM K H, LEE J G, RHEE C K. Growth of isothermally-solidified titanium joints using a multi-component Zr−Ti−Cu−Ni−Be amorphous alloy as a brazing filler [J]. Materials Characterization, 2013, 80: 98−104.

[19] MASSALAKI T B, OKAMOTO H. Binary alloy phase diagrams [M]. Russell Township: ASM International, 1990.

[20] SCHUSTER J C, PAN Zhu, LIU Shu-long, WEITZER F, DU Yong. On the constitution of the ternary system Al−Ni−Ti [J]. Intermetallics, 2007, 15: 1257−1267.
[21] REN Hai-shui, XIONG Hua-ping, CHEN Bo, PANG Shu-jie, CHEN Bing-qing, YE Lei. Vacuum brazing of Ti_3Al-based alloy to TiAl using TiZrCuNi(Co) fillers [J]. Journal of Materials Processing Technology, 2015, 224: 26−32.
[22] DU Sui-geng, WANG Song-lin, DING Ke. A novel method of friction-diffusion welding between TiAl alloy and GH3039 high temperature alloy [J]. Journal of Manufacturing Processes, 2020, 56: 688−696.
[23] ZENG Ke-jun, SCHMID-FETZER R, HUNEAU B, ROGL P, BAUER J. The ternary system Al−Ni−Ti (Part II): Thermodynamic assessment and experimental investigation of polythermal phase equilibria [J]. Intermetallics, 1999, 7: 1347−1359.
[24] RASTKAR A R, SOHI M H. Phase identification and fracture strength of plasma brazed joints of Ti−45Al−2Nb−2Mn−1B with Ti−Ni−Cu filler metals [J]. Materials Letters, 2021, 286: 129249.
[25] REN Hai-shui, REN Xin-yu, XIONG Hua-ping, LI Wen-wen, PANG Shu-jie, USTINOV A I. Nano-diffusion bonding of Ti_2AlNb to Ni-based superalloy [J]. Materials Characterization, 2019, 155: 109813.
[26] de PRADO J, SÁNCHEZ M, RUIZ A, UREÑA A. Effect of brazing temperature, filler thickness and post brazing heat treatment on the microstructure and mechanical properties of W-Eurofer joints brazed with Cu interlayers [J]. Journal of Nuclear Materials, 2020, 533: 152117.
[27] LEE S J, WU S K. Infrared joining strength and interfacial microstructures of Ti−48Al−2Nb−2Cr intermetallics using Ti−15Cu−15Ni foil [J]. Intermetallics, 1999, 7: 11−21.
[28] REN Hai-shui, XIONG Hua-ping, CHEN Bo, PANG Shu-jie, CHEN Bing-qing, YE Lei. Microstructures and mechanical properties of vacuum brazed Ti_3Al/TiAl joints using two Ti-based filler metals [J]. Journal of Materials Science & Technology, 2016, 32: 372−380.
[29] WAN Bao, LI Xiao-qiang, PAN Cun-liang, LI Dong-yu, QU Sheng-guan, YANG Chao. Microstructure and mechanical properties of TiAl/Ni-based superalloy joints vacuum brazed with Ti−Zr−Fe−Cu−Ni−Co−Mo filler metal [J]. Rare Metals, 2021, 40(8): 2134−2142.
[30] LI Yu-xuan, WANG Hou-qin, HAN Ke, LI Xiao-peng, ZHANG Bing-gang. Microstructure of Ti−45Al−8.5Nb−0.2W−0.03Y electron beam welding joints [J]. Journal of Materials Processing Technology, 2017, 250: 401−409.
[31] KATHLEEN M. Fractography [M]. Russell Township: ASM International, 1987.

钎焊温度对微纳米 Ti−Cu−Ni−Nb−Al−Hf 钎料真空钎焊 γ-TiAl 接头组织和抗拉强度的影响

李 力[1,2,3]，陈昱橦[1,2]，袁雷昕[1,2]，罗 芬[1,2]，冯志雪[1,2]，李小强[3]

1. 华东交通大学 材料科学与工程学院，南昌 330013；
2. 华东交通大学 轨道交通基础设施性能监测与防护国家重点实验室，南昌 330013；
3. 华南理工大学 国家金属材料近净成形工程技术研究中心，广州 510640

摘 要：采用自主研制的新型 Ti−10Cu−10Ni−8Al−8Nb−4Zr−1.5Hf 微纳米钎料，在钎焊温度 1160~1220 ℃、钎焊时间 30 min 的工艺参数下真空钎焊连接 Ti−47Al−2Nb−2Cr−0.15B 合金。研究 TiAl 钎焊接头的界面组织和形成机理，以及钎焊温度、界面组织和接头强度之间的内在联系。结果表明，钎焊温度 1160 和 1180 ℃的 TiAl 接头均由三个界面反应层组成，主要物相均为 α_2-Ti_3Al、τ_3-Al_3NiTi_2 和 Ti_2Ni。然而，当钎焊温度为 1200 和 1220 ℃时，由于具有壁垒效应的连续 α_2-Ti_3Al 层被打破，导致钎缝中未见明显分层，τ_3-Al_3NiTi_2 完全取代 Ti_2Ni 且均匀分布在钎缝中。当钎焊温度为 1200 ℃时，钎焊接头的抗拉强度显著提高，最大抗拉强度为 343 MPa。需特别指出的是，在不同钎焊温度下，溶解的 TiAl 母材中向外扩散的 Al 是影响钎焊接头组织演变和抗拉强度的主控因素。

关键词：γ-TiAl 合金；微纳米钎料；真空钎焊；界面显微组织；抗拉强度

(Edited by Xiang-qun LI)